Desalination and Water Treatment
www.deswater.com
doi: 10.5004/dwt.2023.29568

294 (2023) 259–271
May

Assembly of sodium lignosulfonate-metal hybrids as highly efficient adsorbents for rapid removal of dye molecules

Weijun Gao[a,b], Liuyang Wang[a,†], Yun Liu[a,*]

[a]*College of Life Science and Technology, Beijing University of Chemical Technology, Beijing 100029, China, Tel.: +86-10-64421335; Fax: +86-10-64416428; emails: liuyun@mail.buct.edu.cn (Y. Liu), wangliuyang_buct@163.com (L. Wang)*
[b]*China Shenhua Coal to Liquid and Chemical Co., Ltd., Beijing 1000112, China, email: 19691132@qq.com*

Received 12 June 2020; Accepted 15 April 2023

ABSTRACT

This present work describes a pH-driven approach for synthesizing sodium lignosulfonate-metal ions (SL-M) hybrids as highly efficient adsorbent for the rapid removal of dye molecules, including cationic dye (such as Methylene blue, MB), anionic dye (such as Coomassie Brilliant Blue R-250, CBB R-250) and non-ionic dye (such as Rhodamine B, RB). The structural properties of as-synthesized hybrids are characterized using scanning electron microscopy, energy-dispersive X-ray spectroscopy-mapping, Fourier-transform infrared spectroscopy and Brunauer–Emmett–Teller techniques. The adsorption experiments yielded a maximum adsorption capacity of 10,416.51 mg/g of CBB R-250 over SL-Cr^{3+}, 926.97 mg/g of MB over SL-Mn^{2+}, and 880.98 mg/g of RB over SL-Fe^{3+} hybrid at 25°C. The adsorption behavior of SL-M hybrids follows Langmuir isotherm and pseudo-second-order kinetic models well. Thermodynamic studies point out that dye adsorption is spontaneous and endothermic. The dyes adsorption mechanism of SL-M hybrids is probably ascribed to electrostatic interactions, hydrogen bonding, van der Waals forces and π–π stacking interaction. The practical application of SL-M hybrids was demonstrated through the preparation of an SL-M membrane for efficient removal of mixed dyes. Furthermore, the effect of pH and salinity on the dye removal by the SL-M membrane was also investigated. Overall, these findings demonstrate that SL-M hybrids have the potential to serve as an excellent adsorbent for the rapid removal of dyes from polluted water in the future.

Keywords: Sodium lignosulfonate-metal (SL-M) hybrids; Dyes adsorption; Kinetics; Isotherm; Thermodynamics

1. Introduction

Dye molecules, which exist in large quantities in the wastewater discharged from various industrial sections such as textile, dying, tanner, pulp and paper, paint and pigments, are one of the most relevant categories of environmental pollutants [1]. It has been reported that more than 100,000 commercial dyes (including anionic, cationic or non-ionic) with an annual production of approximately $\times 10^6$ tons [2]. The rapid absorptive removal of these organic dyes is a focus of research for the development of sustainable eco-environments, and many efforts are being made to seek low-cost and efficient adsorbents. Among numerous studies, biomass-based adsorbents show good removal percentages and adsorption capacities of dyes due to their low cost and renewable merits [3]. As a renewable and abundant source, lignin-based materials are attracting special attention to complement the greener paradigm for the majority of applications, including air pollutant adsorption (e.g., SO_2, CO_2 and H_2S), heavy metals adsorption (such as Zn, Cu, Cd and Pb), noble metals recovery (e.g., Au, Pt, and Pd), and removal of organic dyes and toxic organics (e.g., Procion

* Corresponding author.
† Equal contributor to this work.

blue MX-R, Methylene blue, and phenols) [4]. In 2019, Supanchaiyamat et al. [4] reviewed an outstanding article on the present trends, perspectives, and opportunities of lignin-based materials. They highlighted lignin's aromatic and three-dimensional structure, which makes it a promising candidate as an adsorbent for removing gases, metals, organics, and dyes.

Lignin, which contains many oxygen functionalities such as phenolic and alcoholic hydroxyl, carbonyl, carboxyl, methoxyl, and ether, is suitable adsorbent in both native and modified forms [5]. For instance, Suteu et al. [6] used industrial lignin as an adsorbent to remove Brilliant Red HE-3B dye with an adsorption capacity of 10.173 mg/g. Zhang et al. [7] studied the use of lignin from steam-exploded rice straw for removal of Methylene blue, achieving a maximum adsorption capacity of 20.38 mg/g. Fu et al. [8] and Kriaa et al. [9] investigated separately the use of activated carbon derived from lignin to adsorb Methylene blue, achieving maximum adsorption capacities of 92.51 and 147 mg/g, respectively. Mahmoudi et al. [10] prepared activated carbon from lignin to adsorb methyl orange dye with a maximum adsorption capacity of 300 mg/g. In addition to activated carbon, lignin-based materials modified through carboxymethylation, acetylation, and sulfomethylation have been used to adsorb different dye molecules, such as Brilliant Red 2BE [11], Procion blue MX-R [12], methyl blue [13], and ethyl violet [14]. These published studies demonstrate the potential of lignin-based adsorbents for the removing dyes from wastewater contaminants in a green chemistry perspective.

To date, studies on lignin as a good adsorbent have mainly focused on kraft lignin, hydrolysis lignin, organosolv lignin as well as their modified carbon materials. As one of the main industrial lignin products, lignosulfonate with sulfonate groups, polyanionic electrolytes, has good water solubility and is rarely directly but composite with other compounds used as adsorbent for removal of dye molecules [15]. For instance, Li et al. [13] prepared SL-M gels through cross-linking sulfomethylated lignin and epichlorohydrin, exhibiting high performance for Methylene blue removal with an adsorption capacity of 495.4 mg/g, five times higher than unmodified kraft lignin (97.22 mg/g). Gu et al. [16] successfully synthesized chitosan–lignosulfonate composite as an excellent adsorbent for Congo red, Rhodamine B, and Cr(VI). However, little information is available on the use of sodium lignosulfonate-metal ions (SL-M) coordination hybrids as excellent adsorbent for dye molecules removal from wastewater in batch and continuous modes. By using this approach, two significant advantages can be obtained: first, lignosulfonate can directly adsorb metal ions to fabricate SL-M coordination complexes through pH-tuning. Second, SL-M coordination complexes can be used to remove dye molecules from polluted water.

To achieve the aforementioned goals, this study presents a straightforward and effective pH-driven approach to synthesizing SL-M hybrid for batch-mode removal of various dye molecules from wastewater. These include cationic dye such as Methylene blue, anionic dye such as Coomassie Brilliant Blue R-250 (CBB R-250), and non-ionic dye such as Rhodamine B. The structural properties of the prepared samples are characterized using many techniques such as scanning electron microscopy (SEM), energy-dispersive X-ray spectroscopy-mapping, Fourier-transform infrared spectroscopy (FT-IR), and Brunauer–Emmett–Teller (BET). Additionally, the adsorption performance of the prepared samples is evaluated through studies of adsorption kinetics, isotherm models and thermodynamics. Simultaneously, the dyes adsorption mechanism over the SL-M adsorbent was briefly proposed. In the end, this study investigates the practical application of the SL-M adsorbent for removing a mixture of dyes and effect of salinity on the dye removal process.

2. Materials and methods

2.1. Materials

Sodium lignosulfonate ($C_{20}H_{24}Na_2O_{10}S_2$, MW = 534.51 g/mol, 96%) was purchased from Sigma-Aldrich Co., Shanghai, China. Methylene blue (cationic dye, $C_7H_7NO_2$, MW = 137.14 g/mol, λ_{max} = 664 nm, MB) was gotten from Kemio Chemical Reagent Co., Ltd., Tianjin, China. Coomassie Brilliant Blue R-250 (anionic dye, $C_{45}H_{44}O_7H_3S_2Na$, MW = 824 g/mol, λ_{max} = 556 nm, CBB R-250) was bought from BIOTOP Co., Beijing, China. Rhodamine B (non-ionic dye, $C_{28}H_{31}C_1N_2O_3$, MW = 479.01 g/mol, λ_{max} = 554 nm, RB) was obtained from AMRESCO Co., Shanghai, China. All other chemicals used in this study were bought from local markets in Beijing. Unless otherwise stated, all chemicals were used directly without further purification.

2.2. Synthesis of sodium lignosulfonate-metal coordination hybrids

The synthesis of SL-M coordination hybrid followed the methods described in our previous works [17,18] and is outlined in Fig. 1. In brief, a 10 mL solution of sodium lignosulfonate with a concentration of 0.8% was placed into a clean 25 mL glass bottle. Then, 2.5 mL of a 20 mmol solution of each metal ion, including $CrCl_3{\cdot}6H_2O$, $MnSO_4{\cdot}H_2O$, $FeCl_3{\cdot}6H_2O$, $Co(NO_3)_2{\cdot}6H_2O$, $Ni(NO_3)_2{\cdot}H_2O$, $CuSO_4{\cdot}H_2O$, and $ZnSO_4{\cdot}H_2O$, was added to the bottle and vigorously stirred at 1,000 rpm for 1 h. Insoluble precipitates of the SL-M coordination hybrid were observed by adjusting the pH of the mixture solution with 10 wt.% aqueous ammonia (0.1 M). After static aging for 12 h, the clear supernatant was discarded, and the SL-M coordination hybrids were obtained by centrifugation at 5,000×g for 10 min, followed by rinsing with deionized water three times to remove unchelated metal ions, and hot air drying at 80°C overnight. The yield of SL-M coordination hybrid was estimated, and its structural properties were characterized.

2.3. Characterization and analysis methods

The FT-IR analysis was conducted using a Bruker Tensor 27 FT-IR spectrometer (Bruker BioSciences Co., German) in the range of 4,000–400 cm^{-1} through the KBr disk method. The morphologies and element mapping were characterized using a Hitachi S-4700 scanning electron microscopy (SEM, Japan) equipped with energy-dispersive X-ray spectroscopy (EDX) at 10 kV. The Micromeritics ASAP 2460 instrument (USA) was used to obtain nitrogen adsorption–desorption

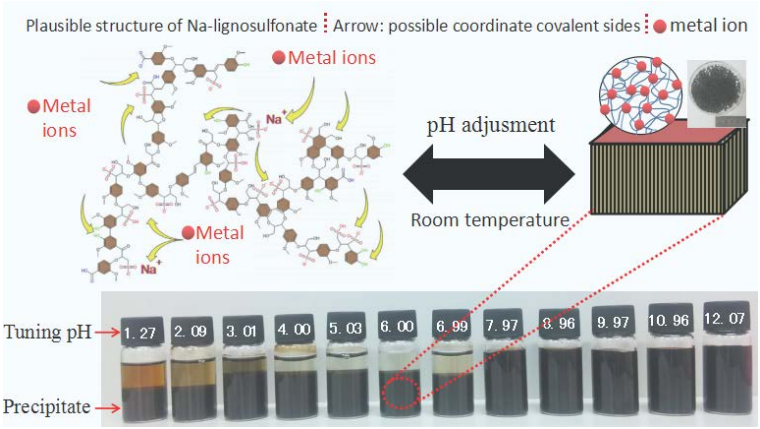

Fig. 1. An overview of the synthesis procedure of SL-M coordination hybrids, which involves tuning the pH. As an example, the synthesis of SL-Cr^{3+} coordination hybrid is examined under various pH conditions.

isotherms, which were used to determine the BET surface and pore size. The samples were degassed at 250°C for 12 h before measurement. The concentration of dye molecules was determined by monitoring the optical density (OD) absorbance value using an UV756CRT UV-Vis Spectrophotometer (Shanghai Yoke Instrument Co., Ltd., Shanghai, China). The adsorption capacity and removal percentage of dye molecules were calculated based on the difference in absorbance.

2.4. Adsorption experiments

Batch adsorption experiments were conducted at room temperature (25°C) following the methods reported by Siqueira et al. [19]. The tested dye molecules (CBB R-250, RB, MB) were dissolved in deionized water to obtain a stock solution with the concentration of 1.0 mg/mL. A fixed amount (0.1 mg/mL) of the SL-M coordination hybrid was added into 5 mL of dye solution with an initial concentration ranging from 0.005 to 0.6 mg/mL. The solution was then shaken in a temperature-controlled water bath shaker (SHZ-82A, China) until adsorption equilibrium was reached. The equilibrium concentration of the dye molecules in the solution was measured using a UV756CRT UV-Vis Spectrophotometer (Shanghai Yoke Instrument Co., Ltd., Shanghai, China). The amount of dyes adsorbed on the SL-M coordination hybrid and the removal percentage of dyes at equilibrium were calculated using Eqs. (1) and (2), respectively.

$$q_e = \frac{\left(C_0 - C_e\right) \times V}{m} \tag{1}$$

$$\text{Removal}(\%) = \frac{\left(C_0 - C_e\right)}{C_0} \times 100\% \tag{2}$$

where q_e is the adsorbed amount of dye at equilibrium, mg/g; c_0 and c_e are the initial and equilibrium concentration of dye, respectively, mg/L; V represents the volume of dye solution, L; m is the mass weight of SL-M coordination, g.

The kinetics of dye adsorption onto the SL-M coordination hybrid under batch mode were analyzed using pseudo-first-order and pseudo-second-order equations [19], which are represented as Eqs. (3) and (4), respectively.

$$\log\left(q_e - q_t\right) = \log q_e - k_1 t \tag{3}$$

$$\frac{1}{q_t} = \frac{1}{k_2 q_e^2} + \frac{t}{q_e} \tag{4}$$

where q_t and q_e is the amount of dye adsorbed at time t and equilibrium, respectively, mg/g; k_1 is the pseudo-first-order rate constant (min^{-1}); k_2 is the pseudo-second-order rate constant (g/mg·min).

To investigate the adsorption behavior of the dye at equilibrium, we employed the Langmuir isotherm model [20] and Freundlich isotherm model [21], which were represented as Eqs. (5) and (6), respectively.

$$\frac{C_e}{q_e} = \frac{1}{q_{\max} k_L} + \frac{C_e}{q_{\max}} \tag{5}$$

$$q_e = k_F C_e^{1/n} \tag{6}$$

where q_e is the amount of dye adsorbed on the synthesized sample at equilibrium, mg/g; C_e is the dye concentration at equilibrium, mg/L; $q_{\max}$ is the maximal adsorption capacity, mg/g; k_L is Langmuir adsorption equilibrium constant mg/g; k_F (L/mg) and n are Freundlich constants.

To calculate the thermodynamic parameters of adsorption, namely the Gibbs free energy (ΔG°), standard enthalpy change (ΔH°) and standard entropy change (ΔS°), we used Eqs. (7) and (8), given as:

$$\Delta G^\circ = -RT \ln K_C \tag{7}$$

$$\ln K_C = \frac{\Delta S^\circ}{R} - \frac{\Delta H^\circ}{RT} \tag{8}$$

where R is the universal gas constant, 8.314 J/mol·K; T is the absolute temperature, K; K_C is the thermodynamic equilibrium constant and was calculated by Sips isotherm equation [19].

2.5. Preparation of SL-M membrane for mixture dyes removal

As illustrated in Fig. 1, the coordination structure of the SL-M hybrids is significantly affected by the pH of the solution. Therefore, this study does not include experiments on the desorption and regeneration of SL-M hybrids as adsorbents. However, to investigate the practical applications of SL-M hybrids, we prepare an SL-M filtering membrane for mixture dyes removal. In detail, 200 mg of SL-M hybrids and 1 g of chitosan were dissolved into 50 mL of water containing 0.2% acetic acid, and polyurethane (PU) foam measuring 25 mm × 100 mm was completely immersed into the mixture solution for 12 h. Subsequently, the PU foam was drawn out and compressed into a flake with a diameter of 2.5 cm and a thickness of 1.0 mm. This flake can be used as a filter membrane for dyes filtering. In this section, we conducted two experiments: (1) using SL-M membrane to remove a mixture of dyes such as CBB R-250/MB, MB/RB, CBB R-250/RB, and CBB R-250/MB/RB; (2) studying the effect of pH (pH = 6, 7, 8, and 9) and salinity (1, 3 and 5 g/L) on dyes' removal efficiency through the SL-M membrane.

3. Results and discussion

3.1. Synthesis of SL-M coordination hybrid and screening for dyes adsorption

Fig. 2a illustrates the synthesis of seven SL-M coordination hybrids, namely SL-Cr^{3+}, SL-Mn^{2+}, SL-Fe^{3+}, SL-Co^{2+}, SL-Ni^{2+}, SL-Cu^{2+}, SL-Zn^{2+}, under optimal pH conditions. The yield of SL-M coordination hybrids ranges from 31.2% to 80.9% within the suitable pH range (are shown in Fig. 2b). The formation of SL-M coordination precipitant is attributed to the chelation of metal ions with the phenolic hydroxyl group in SL [17,18,22,23]. Clearly, the formation of SL-M coordination hybrids is significantly dependent on solution pH. Interestingly, these coordination polymers exhibit a reversible pH-driven transformation. Under low and high pH conditions, SL-M coordination can transform into their dissolved forms and returned to their precipitant form in suitable pH conditions (as depicted in Fig. 2c).

In order to identify an excellent candidate adsorbent, all seven as-prepared SL-M coordination hybrids were screened for their ability to adsorb three different dye molecules: CBB R-250 (representing anionic dye), MB (representing cationic dye) and RB (representing non-ionic). Adsorption experiments were conducted using dye concentrations of 0.02 mg/mL, an adsorbent loading of 0.02 mg/mL, a temperature of 25°C, a total volume of 5 mL, and a contact time of 3 h. The adsorption capacities of the SL-M coordination hybrid were calculated using the Langmuir adsorption equation and the results are shown in Fig. 3.

Based on the data, SL-Cr^{3+} showed the highest adsorption performance for CBB R-250 removal, with an impressive capacity of 10,416.51 mg/g. SL-Mn^{2+} demonstrated a high adsorption capacity of MB, with a value of 926.97 mg/g, while SL-Fe^{3+} exhibited excellent adsorption of RB, with a value of 880.98 mg/g. These maximum dye molecules capacities for SL-Cr^{3+}, SL-Mn^{2+} and SL-Fe^{3+} far exceed the values reported by native lignin and its modified materials [5–16]. For instance, SL-M gels derived from sulfomethylated lignin and epichlorohydrin were reported as highly efficient adsorbents for MB removal, with an adsorption capacity of 495.4 mg/g [13]. Overall, the results suggest that SL-Cr^{3+} coordination hybrid is a promising and efficient adsorbent candidate for removing CBB R-250c dye, SL-Mn^{2+} is suitable for MB dye removal, and SL-Fe^{3+} is a potential candidate for RB dye removal from wastewater in the future.

3.2. Structural properties of SL-Cr^{3+}, SL-Mn^{2+} and SL-Fe^{3+} coordination hybrids

FT-IR was used to investigate the interaction between lignosulfonate and metal ions (SL-Cr^{3+}, SL-Mn^{2+} and SL-Fe^{3+}) in coordination hybrids. The hybrids were formed

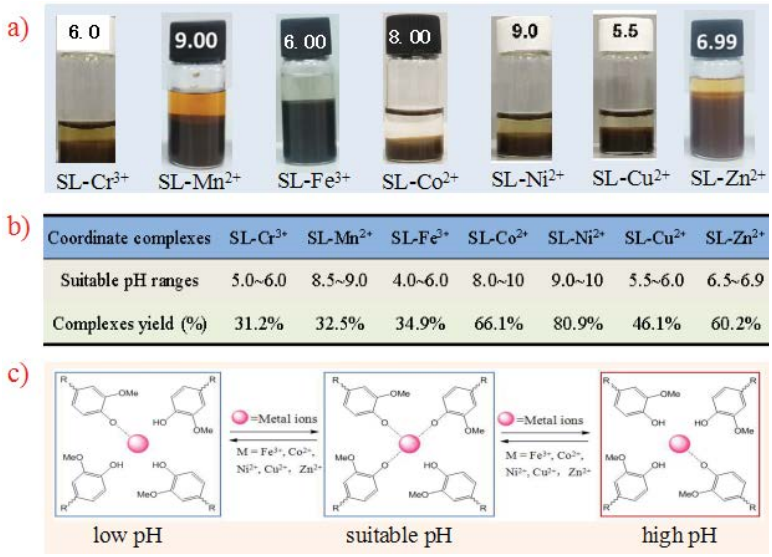

Fig. 2. Formation of SL-M coordination hybrids can be achieved through pH adjustment, which affects the suitable pH (a), yield (b) and assembly mechanism (c) of these hybrids.

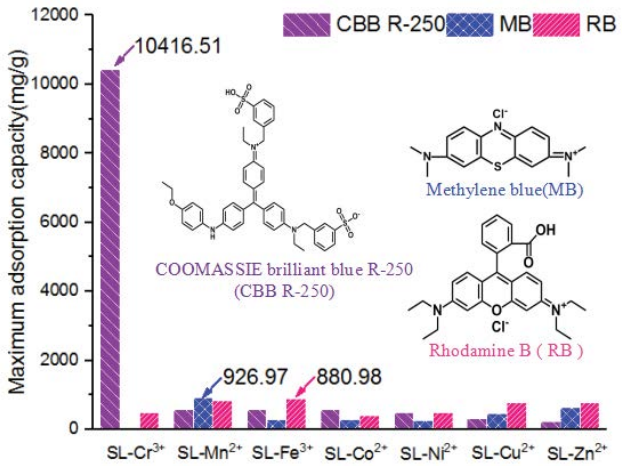

Fig. 3. A screening of SL-M coordination hybrid as an adsorbent for the efficient removal of dye molecules of CBB R-250, Methylene blue and Rhodamine B at room temperature, using the following conditions: dye concentration of 0.02 mg/mL, adsorbent loading of 0.1 mg, temperature of 25°C, total volume of 5 mL, and a duration of 3 h.

through strong covalent chelate groups, which were confirmed by the FT-IR spectra (Fig. 4a).

The FT-IR characteristic peaks of lignin reported in the literature [24–26] showed that the bands at 2,847; 1,513 and 1,053 cm^{-1} in the FT-IR spectra of SL-M coordination have lower intensity than native SL, possibly due to the formation of metal (Cr^{3+}, Mn^{2+} and Fe^{3+}) phenolates and carboxylates. In contrast, the bands at 1,602; 1,471 and 1,431 cm^{-1} showed increased intensity after the addition of metal ions (Cr^{3+}, Mn^{2+} and Fe^{3+}), indicating the inclusion of metal ions between the unconjugated carbonyl–carboxyl and sulfonate. Additionally, the increases in C–H deformations at 1,145; 1,088 and 862 cm^{-1} were also observed upon the addition of metal ions (Cr^{3+}, Mn^{2+} and Fe^{3+}). The EDX profiles (Fig. 4b–d) were used to detect the contents of metal ions in SL-Cr^{3+}, SL-Mn^{2+} and SL-Fe^{3+} coordination hybrids, and the atom percentages of Cr^{3+}, Mn^{2+} and Fe^{3+} were found to be 1.54, 1.18 and 0.60 at.%, respectively (Fig. 4b–d).

Fig. 5 displays the nitrogen adsorption curves obtained from the BET measurement, which reveals that the particle pore sizes of SL-Cr^{3+}, SL-Mn^{2+} and SL-Fe^{3+} coordination hybrids are 2.30 nm, 4.88 nm, and 7.59 nm, respectively. However, the surface areas of the three SL-M coordination

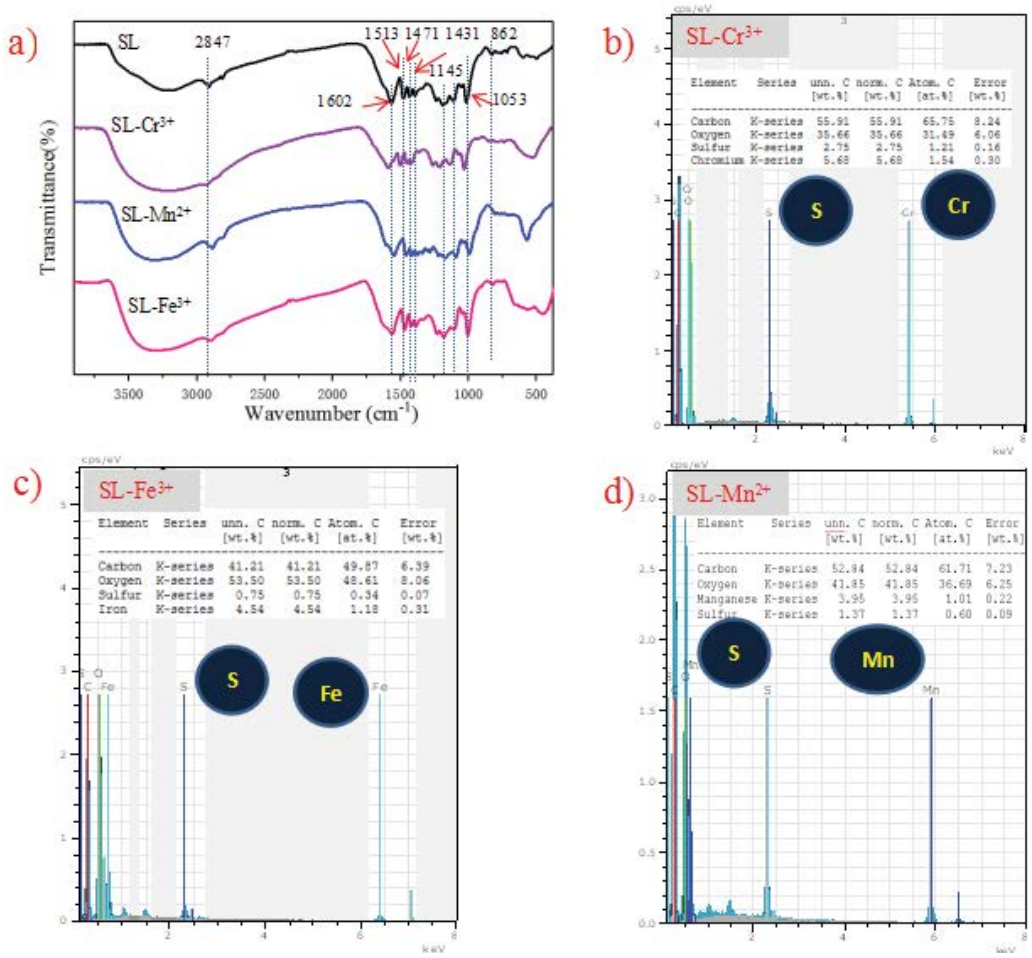

Fig. 4. Fourier-transform infrared spectroscopy (a) and energy-dispersive X-ray spectroscopy profiles (b–d) of SL, SL-Cr^{3+}, SL-Mn^{2+} and SL-Fe^{3+} coordination hybrids.

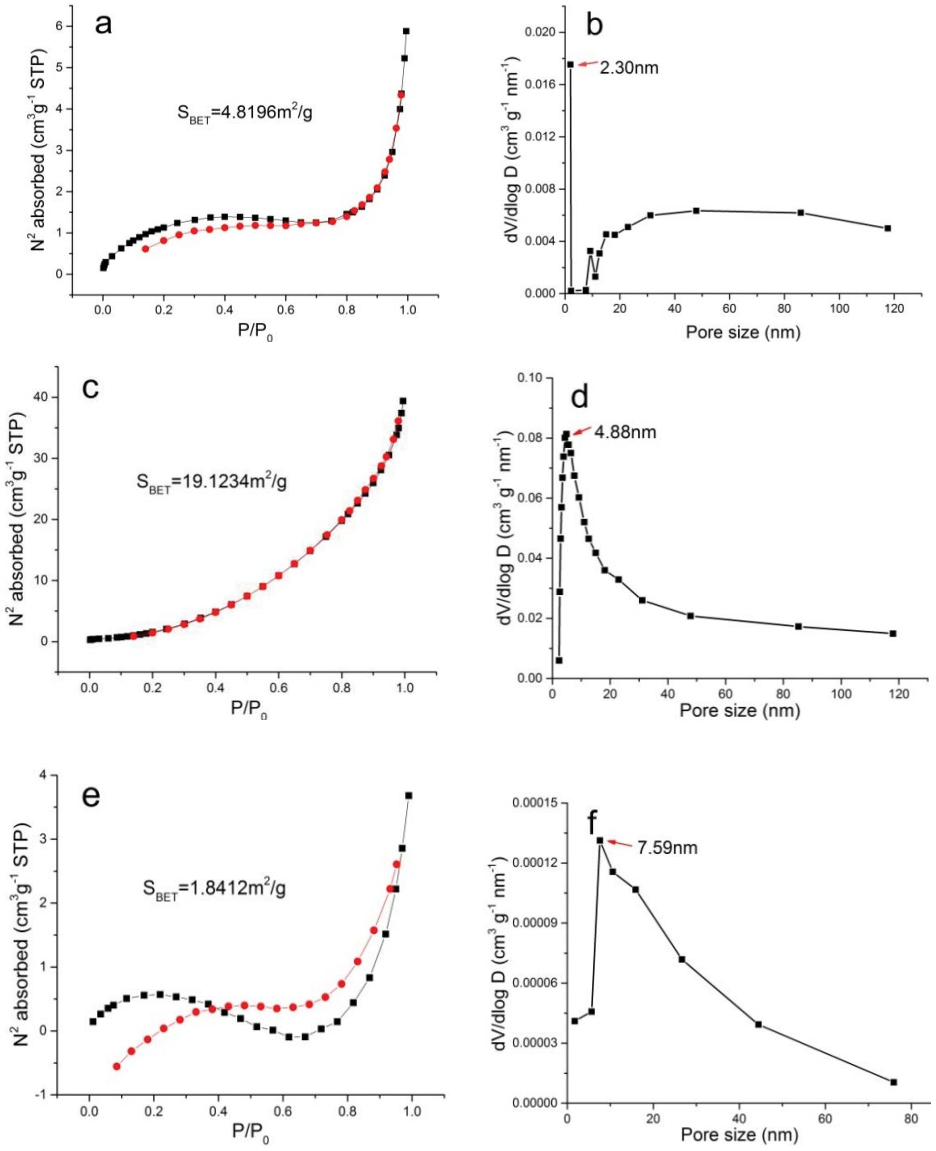

Fig. 5. Brunauer–Emmett–Teller surface area of SL-Cr^{3+} (a), SL-Mn^{2+} (c), SL-Fe^{3+} (e) coordination calculated from the N_2 adsorption isotherm, and P and P_0 are the equilibrium and saturation pressures of N_2 at 77 K, respectively. The mesoporous structures of SL-Cr^{3+} (b), SL-Mn^{2+} (d), SL-Fe^{3+} (f) coordination obtained by Barrett–Joyner–Halenda analysis.

complexes obtained from the BET data are very small (ranging from 1.84 to 19.12 m^2/g), probably due to structural collapse during freeze-drying. This suggests that while the structure of SL-Cr^{3+}, SL-Mn^{2+} and SL-Fe^{3+} coordination hybrid remains stable in solution state, it may be damaged under dried conditions.

The SEM images clearly show differences in the surface morphology of SL-M coordination hybrids before and after the adsorption of dye molecules. Prior to adsorption, the surface of SL-Cr^{3+}, SL-Mn^{2+} and SL-Fe^{3+} coordination hybrids are rough with "rod-like" morphology (Fig. 6a, c and e). However, after adsorption, the surface of coordination becomes denser with a "cake-like" morphology, and some clumps are visible (Fig. 6b, d and f). This indicates that the SL-M coordination hybrid has adsorbed dye molecules, which is further confirmed by SEM-mapping chemical elements analyses. The presence of nitrogen elements on the surface of SL-M coordination after adsorption of dye molecules is clearly shown.

3.3. Adsorption kinetics of dyes over SL-Cr^{3+}, SL-Mn^{2+} and SL-Fe^{3+} coordination

The time-dependent kinetic studies for the batch-wise adsorption of CBB R-250 onto SL-Cr^{3+}, MB onto SL-Mn^{2+}, and RB onto SL-Fe^{3+} coordination hybrid showed a remarkably fast removal rate, with adsorption equilibrium achieved within 30 s as measured by UV-Vis spectroscopy (Fig. 7). The nearly instantaneous adsorption observed in this study is likely due to the three-dimension network structure with hierarchical mesoporosity of SL-M coordination hybrids. The results are consistent with the findings reported by Maleki et al. [24] who observed rapid removal of organic

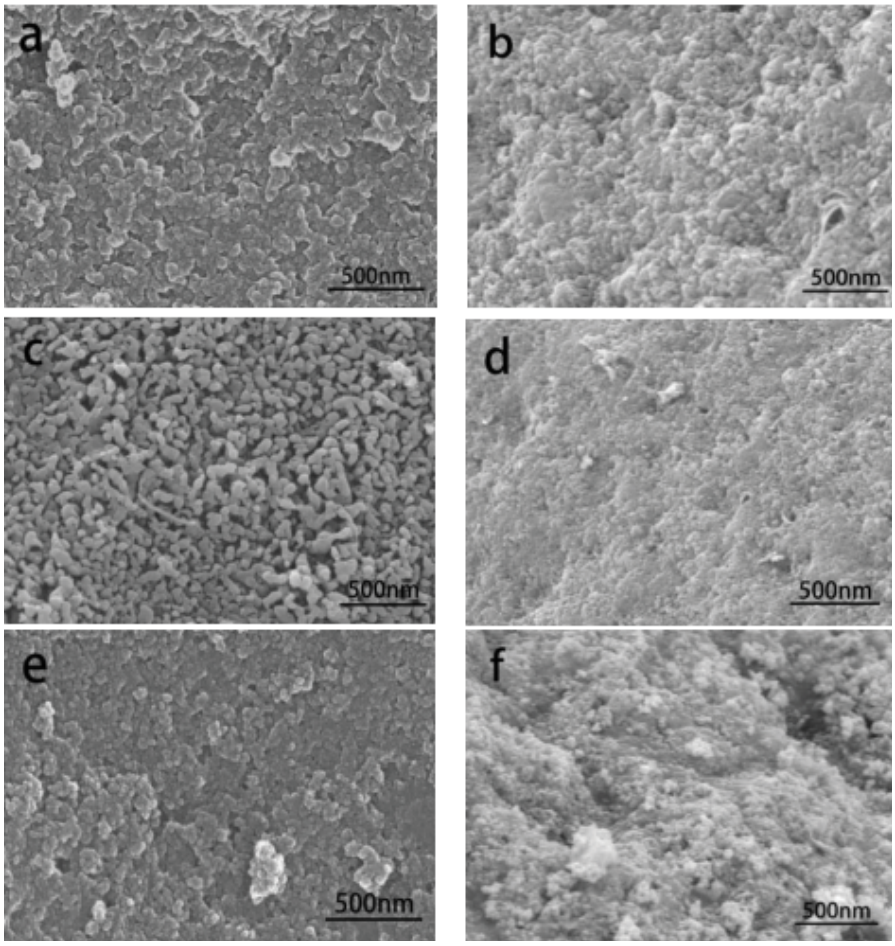

Fig. 6. Scanning electron microscopy images of SL-Cr^{3+} coordination (a), and its adsorption of CBB R-250 (b), as well as SL-Mn^{2+} coordination (c), and its adsorption of Methylene blue (d), and SL-Fe^{3+} coordination (e), and its adsorption of Rhodamine B (f).

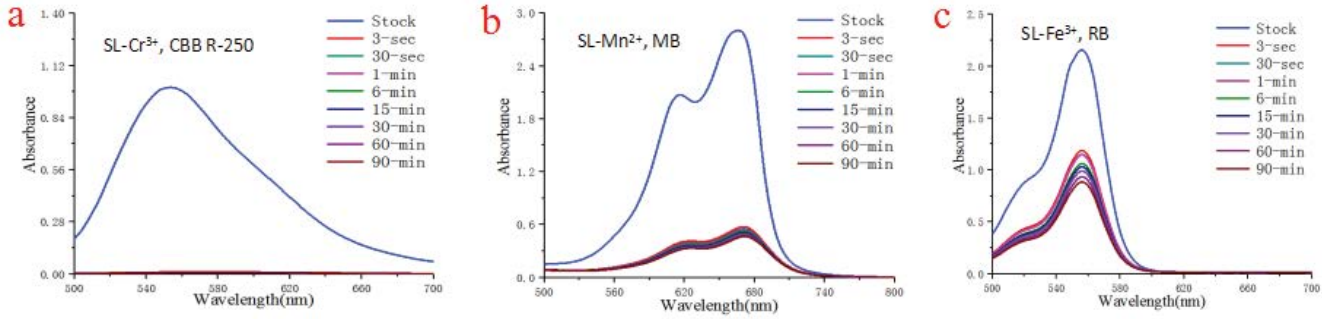

Fig. 7. The time-dependent kinetics of dyes (0.02 mg/mL) adsorption onto SL-Cr^{3+}, SL-Mn^{2+}, and SL-Fe^{3+} coordination hybrids, with an adsorbent loading of 0.1 mg, a sample volume of 5 mL, and a contact time of 0–90 min at a temperature of 25°C and a stirring rate of 150 rpm. The pH was adjusted to a suitable value, pH = 6.0 for SL-Cr^{3+} and SL-Fe^{3+}, and pH = 9.0 for SL-Mn^{2+}.

micropollutants from water using a porous β-cyclodextrin polymer.

Fig. 8 shows the adsorption kinetics data fitted into both pseudo-first-order and pseudo-second-order equations, and Table 1 depicts the obtained parameters. As observed from the results presented in both the figure and the table, the pseudo-second-order equation exhibits better agreement between the experimental and calculated values, and also shows a higher correlation coefficient ($R^2 \geqq 0.997$) compared to the pseudo-first-order equation. These findings suggest that the adsorption kinetics data of dye molecules onto SL-M coordination hybrids are better modeled by the pseudo-second-order equations, indicating that chemo-adsorption may be the rate-controlling step for this adsorption process.

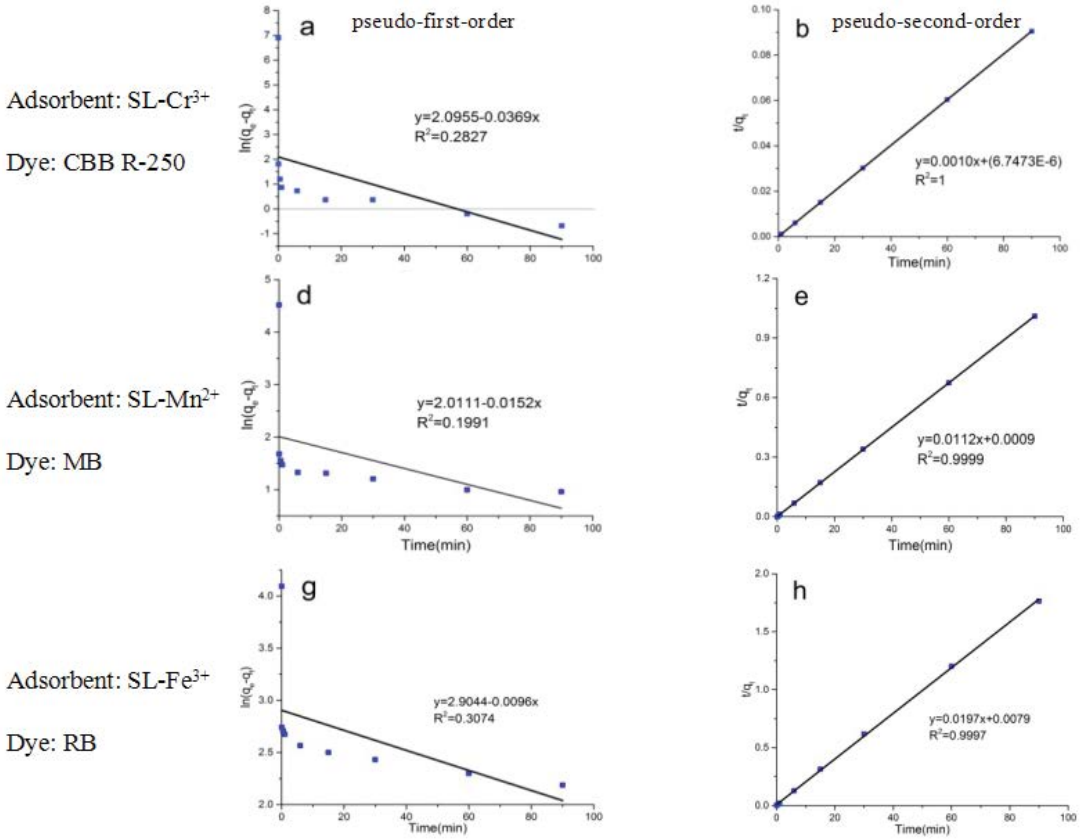

Fig. 8. Kinetics equations describing the adsorption of dye molecules (CBB R-250, Methylene blue, Rhodamine B) onto coordination hybrids of SL-Cr^{3+}, SL-Mn^{2+} and SL-Fe^{3+}. The pseudo-first-order model is represented by (a,d,g), while the pseudo-second-order model is represented by (a,b,e,h).

Table 1
Adsorption kinetics parameters calculated from pseudo-first-order and pseudo-second-order equations

Adsorbent/dye	Experimental	Pseudo-first-order			Pseudo-second-order		
SL-Cr^{3+}/CBB R-250	q_e (mg/g)	$q_{e,cal}$ (mg/g)	k_1 (min^{-1})	R^2	$q_{e,cal}$ (mg/g)	k_2 (min^{-1})	R^2
	994.49	813.0	0.037	0.2827	1000	0.148	1.0000
SL-Mn^{2+}/MB	q_e (mg/g)	$q_{e,cal}$ (mg/g)	k_1 (min^{-1})	R^2	$q_{e,cal}$ (mg/g)	k_2 (min^{-1})	R^2
	94.38	74.7	0.035	0.1991	89.285	0.139	0.9999
SL-Fe^{3+}/RB	q_e (mg/g)	$q_{e,cal}$ (mg/g)	k_1 (min^{-1})	R^2	$q_{e,cal}$ (mg/g)	k_2 (min^{-1})	R^2
	51.01	18.25	0.022	0.3074	50.761	0.049	0.9970

This observation is consistent with earlier reports on bio-adsorbents derived from biomass in the literature [19].

3.4. Adsorption isotherm of dyes over SL-Cr^{3+}, SL-Mn^{2+} and SL-Fe^{3+} coordination

To investigate the effect of temperature on adsorption process, adsorption isotherm plots were generated at 278.15, 298.15 and 318.15 K, as shown in Fig. 9. Additionally, data obtained at 298.15 K were fitted using Langmuir and Freundlich isotherm models, as presented in Fig. 10.

The concentration of CBB R-250 ranged from 0.005 to 0.02 mg/mL, while the concentration of MB ranged from 0.005 to 0.06 mg/mL, and the concentration of RB ranged from 0.005 to 0.012 mg/mL. The adsorbent loading was kept constant at 0.1 mg/mL and the sample volume was 5 mL. The contact time ranged from 0 to 90 min, and the stirring rate was 150 rpm. pH adjustment to suitable value, pH = 6.0 for SL-Cr^3 and SL-Fe^{3+}, pH = 9.0 for SL-Mn^{2+}.

The results depicted in Fig. 10 and Table 2 indicate that Langmuir isotherm model (R^2 = 0.953~0.996) predicts the adsorption behavior of dye molecules onto SL-Cr^{3+}, SL-Mn^{2+} and SL-Fe^{3+} coordination hybrids more accurately than Freundlich isotherm model (R^2 = 0.816~0.987). This is because R^2 is a critical factor that determines the best-fitted adsorption model [25]. The monolayer adsorption of dye molecules

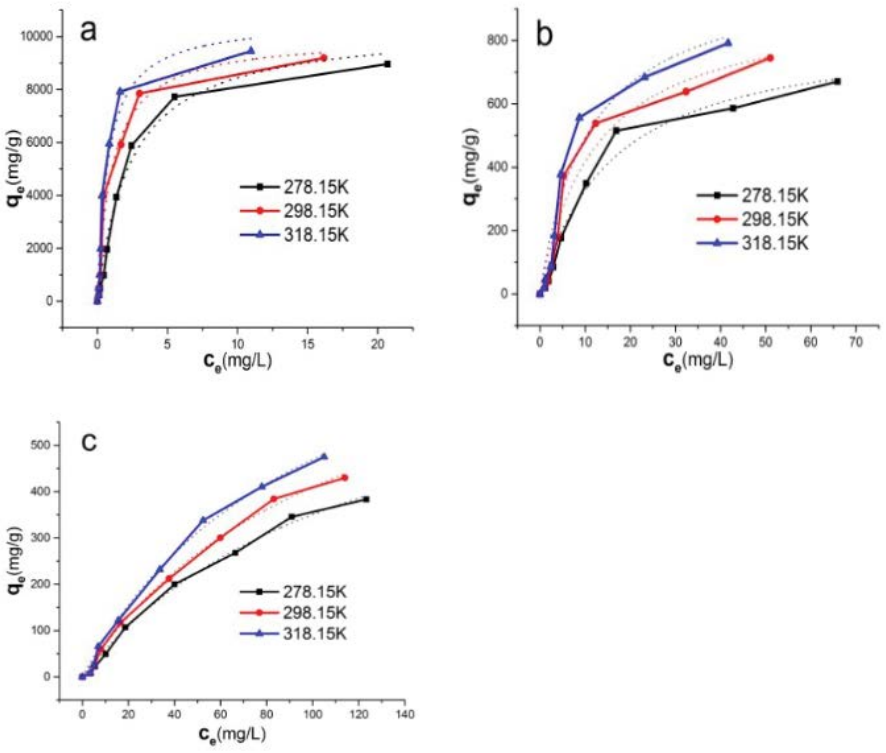

Fig. 9. Isothermal absorption curves of CBB R-250, Methylene blue and Rhodamine B by SL-Cr^{3+} (a), SL-Mn^{2+} (b), and SL-Fe^{3+} (c) coordination complexes at 278.15, 298.15 and 318.15 K.

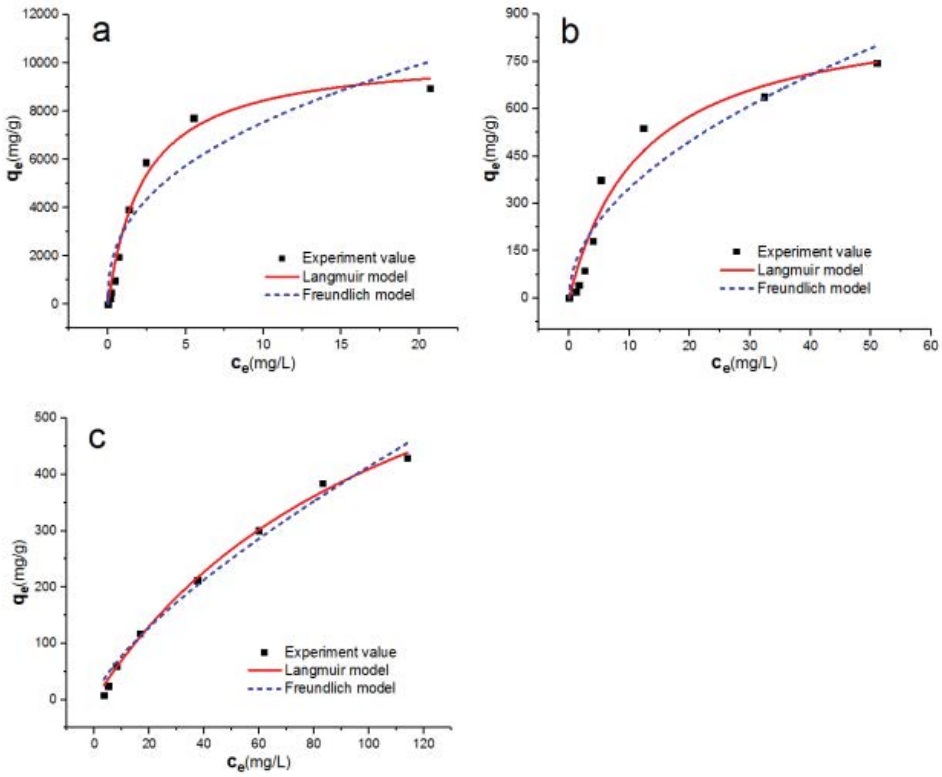

Fig. 10. Isothermal absorption curves of CBB R-250, Methylene blue and Rhodamine B by SL-Cr^{3+} (a), SL-Mn^{2+} (b), and SL-Fe^{3+} (c) coordination hybrids at 298.15 K, which have been fitted with both Langmuir and Freundlich models.

Table 2
Calculated parameters for both Langmuir isotherm adsorption model and Freundlich isotherm model

Adsorbent	Dye molecular	T (K)	Langmuir isotherm model			Freundlich isotherm model		
			Q_m (mg/g)	k_L (L/mg)	R^2	k_F	n	R^2
		278.15	10001.29	0.4279	0.9774	3041.73	2.533	0.8773
SL-Cr^{3+} coordination	CBB R-250	298.15	10416.51	0.9607	0.9832	3934.65	2.892	0.8579
		318.15	10608.40	1.3212	0.9643	4576.91	2.873	0.8159
		278.15	839.94	0.0640	0.9743	89.25	1.9968	0.9156
SL-Mn^{2+} coordination	Methylene blue	298.15	926.97	0.0820	0.9534	108.13	1.965	0.8982
		318.15	1022.00	0.0929	0.9532	125.76	1.932	0.8936
		278.15	777.69	0.0082	0.9956	12.36	1.378	0.9852
SL-Fe^{3+} coordination	Rhodamine B	298.15	883.64	0.0087	0.9962	14.64	1.378	0.9874
		318.15	952.76	0.0097	0.9956	17.22	1.381	0.9848

is assumed by the three SL-M coordination hybrids. The Q_m values increase with the rise in temperature, including the endothermic nature of the adsorption process. The maximum monolayer adsorption capacity of SL-Cr^{3+} for CBB R-250 is 10,416.51 mg/g, SL-Mn^{2+} for MB is 926.97 mg/g, and SL-Fe^{3+} for RB is 880.98 mg/g at 298.15 K. These values are significantly higher than those reported in the literature for other biomass-based adsorbents [5–16]. The probable reason for this is the 3D network structure of SL-M, which enhance dyes adsorption [18], and sulfonation group, which aids in the adsorption process via electrostatic interactions and π–π stacking function [13,22].

3.5. Adsorption thermodynamics of dyes over SL-Cr^{3+}, SL-Mn^{2+} and SL-Fe^{3+} coordination hybrid

Table 3 presents the thermodynamic parameters of adsorption, including the Gibbs free energy ($\Delta G°$), enthalpy ($\Delta H°$), and entropy ($\Delta S°$). The negative value of $\Delta G°$ observed with increasing temperature suggests that the adsorption process is spontaneous and becomes more favorable at higher temperatures. The positive value of $\Delta H°$ indicates an endothermic adsorption and suggests that the adsorption is slightly favored at higher temperatures. Moreover, the negative value of entropy $\Delta S°$ indicates that the dye molecules show reduced randomness at the solid/solution interface during adsorption onto SL-M coordination hybrids. These results suggest that some structural changes may not only occur on the surface of coordination, which was confirmed by SEM surface changes of SL-M coordination before and after adsorption (Fig. 6).

Table 3
Calculated thermodynamic parameters for the adsorption of CBB R-250, Methylene blue and Rhodamine B onto SL-Cr^{3+}, SL-Mn^{2+} and SL-Fe^{3+} coordination hybrids, respectively

SL-M/dye	T (K)	278.15	298.15	318.15
SL-Cr^{3+}/ CBB R-250	$\Delta G°$ (kJ/mol)		–15.724	
	$\Delta H°$ (kJ/mol)	–14.039	12.748	–17.881
	$\Delta S°$ (kJ/mol·K)		–0.096	
SL-Mn^{2+}/ MB	$\Delta G°$ (kJ/mol)		–6.467	
	$\Delta H°$ (kJ/mol)	–5.363	11.487	–17.881
	$\Delta S°$ (kJ/mol·K))		–0.061	
SL-Fe^{3+}/RB	$\Delta G°$ (kJ/mol)		–3.291	
	$\Delta H°$ (kJ/mol)	–2.622	6.913	–3.993
	$\Delta S°$ (kJ/mol·K))		–0.034	

3.6. Mechanism for the adsorption of dyes over SL-Cr^{3+}, SL-Mn^{2+} and SL-Fe^{3+} coordination

The mechanism of dye molecules adsorption over SL-Cr^{3+}, SL-Mn^{2+} and SL-Fe^{3+} coordination hybrids was investigated, and the results are presented in Fig. 11. The coordination assembly of SL-M hybrids involves the hydroxyl functional groups in lignin with metal ions, which act as coordination centers. This leads to the formation of a complex that can adsorb dye molecules from an aqueous solution. The SL-M hybrids can adsorb dye molecules through several mechanisms, including electrostatic interactions, hydrogen bonding, van der Waals forces and π–π stacking interaction, as illustrated in Fig. 11. Anionic dyes with a relatively large nonpolar aromatic part tend to be adsorbed by the phenolic network due to π–π stacking interaction, while cationic dyes can be adsorbed through electrostatic attraction. Non-ionic dyes can be adsorbed by hydrogen bonding and van der Waals forces [26]. The efficiency of the adsorption process depends on various factors such as the pH of the solution, initial dye concentration, temperature and dye molecules structure. In general, the adsorption of dyes over SL-M coordination hybrids is a highly efficient and eco-friendly method for the removal of dyes from wastewater. The method can be easily adapted to different types of dye molecules and can be used as a standalone or combined with other treatment methods.

3.7. Preparation of SL-M membrane for mixture dyes removal

In order to evaluate the effectiveness of the SL-M membrane in removing a mixture of dyes, including CBB R-250/MB, MB/RB, CBB R-250/RB, and CBB R-250/MB/RB, from wastewater, four kinds of mixture dyes were tested. The results, illustrated in Fig. 12, indicate that the SL-M membrane can efficiently remove these dye mixtures. Specifically,

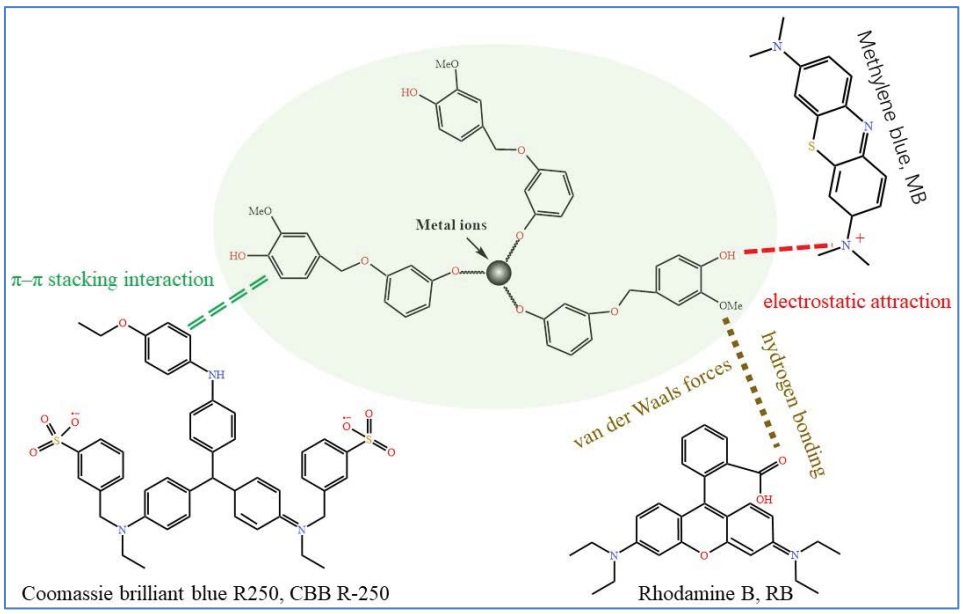

Fig. 11. Proposal mechanism for the adsorption of dyes over SL-M coordination hybrids.

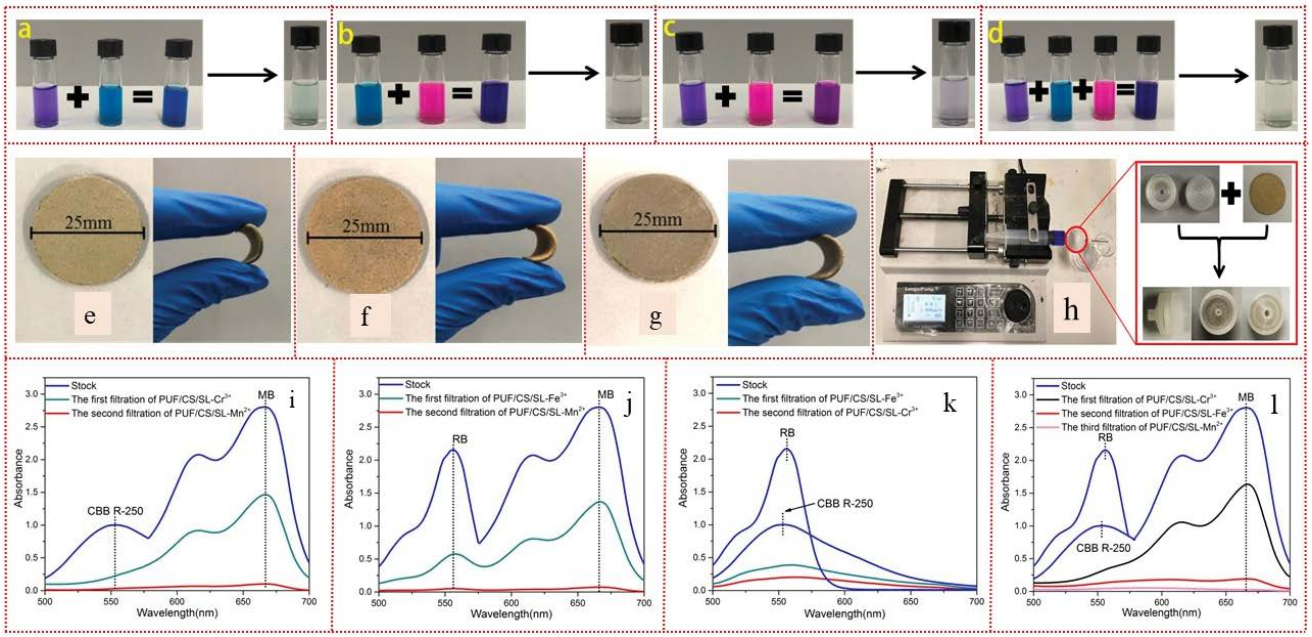

Fig. 12. Performance of the SL-M membrane in removing mixtures of different dyes. (a) CBB R-250/MB mixture, (b) MB/RB mixture, (c) CBB R-250/RB mixture, (d) CBB R-250/MB/RB mixture, (e) SL-Cr^{3+} membrane, (f) SL-Mn^{2+} membrane, (g) SL-Fe^{3+} membrane, (h) membrane filtering set-up, (i) removal of CBB R-250/MB, (j) removal of MB/RB, (k) removal of CBB R-250/RB, and (l) removal of CBB R-250/MB/RB.

the mixture of CBB R-250 and MB dyes was filtered through the SL-Cr^{3+} and SL-Mn^{2+} membranes, resulting in a filtration solution with an absorbance close to zero (Fig. 12i). Likewise, the mixture of MB and RB dyes was effectively removed using the SL-Fe^{3+} and SL-Mn^{2+} membranes (Fig. 12j), while the mixture of CBB R-250 and RB dyes was removed using a combination of the SL-Cr^{3+} and SL-Fe^{3+} membranes (Fig. 12k). Finally, the mixture of CBB R-250, MB, and RB dyes was filtered using the SL-Cr^{3+}, SL-Mn^{2+}, and SL-Fe^{3+} membranes sequentially, resulting in a filtration solution with almost zero absorbance (Fig. 12l). These results suggest that the adsorption effect of the SL-M membrane on mixed dyes is significant.

The effect of pH and salinity on dye removal by the SL-M membrane was investigated, given that dye-containing wastewater is a complex mixture. The results, presented

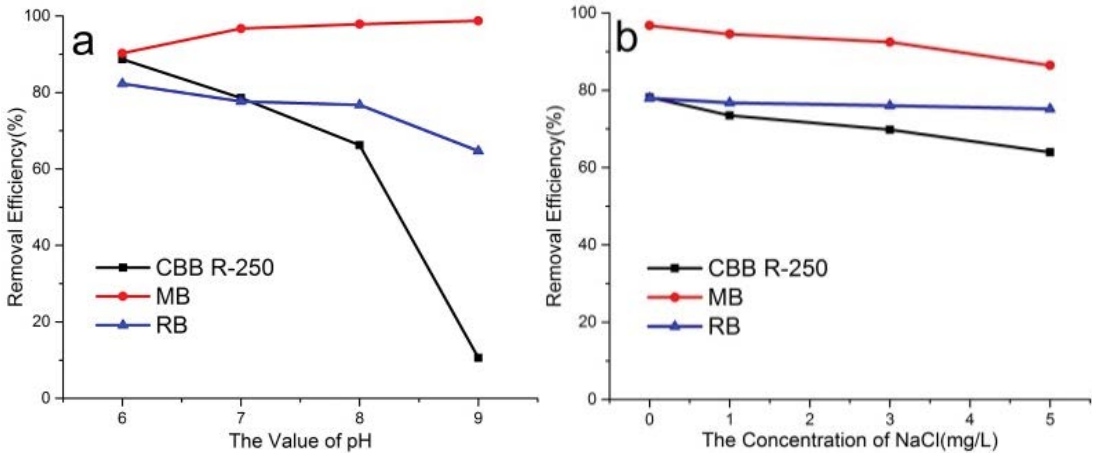

Fig. 13. Effect of pH (a) and salinity (b) on dyes removal by the SL-M membrane.

in Fig. 13a, indicate that the pH of the solution significantly affects the adsorption performance of the SL-M membrane for dye mixtures. Specifically, the pH value has little effect on the performance of the SL-Mn^{2+} membrane in adsorbing MB, with a removal rate of over 90%. However, for the SL-Cr^{3+} membrane and its adsorption of CBB R-250, and for the SL-Fe^{3+} membrane and its adsorption of RB, the adsorption rates decreased with an increase in pH value. Notably, when the pH value was between 8 and 9, the adsorption rate dropped sharply. This can be attributed to the increase in negative charge in the solution with an increase in pH value, resulting in competition with the dye adsorption site and a decrease in the adsorption rate. Our study showed that salinity content had no significant effect on dye removal, as demonstrated by Fig. 13b. Specifically, when the salinity content ranged from 0 to 5 g/L, SL-Mn^{2+} membrane removed more than 87% of MB dye, SL-Fe^{3+} membrane removed over 75% of RB dye, and SL-Cr^{3+} membrane could remove more than 62% of CBB R-250.

4. Conclusion

In summary, this study presents a promising approach for synthesizing SL-M hybrids as efficient adsorbents for the removal of various types of dyes from polluted water. The structural and adsorption properties of the hybrids were characterized, and the adsorption mechanism was suggested to involve various interactions. The practical application of SL-M hybrids was demonstrated through the preparation of a membrane for efficient removal of mixed dyes, and the effect of pH and salinity on dye removal was investigated. These findings suggest that SL-M hybrids could be a potential solution for the treatment of dye-contaminated water. Further research could focus on optimizing the synthesis and performance of SL-M hybrids and investigating their potential applications in large-scale water treatment processes. Additionally, the study highlights the importance of considering the effect of pH and salinity on the performance of the SL-M membrane, which could lead to further investigations into the use of these materials in challenging water treatment scenarios.

Author contributions

"Conceptualization, supervision, writing—review and editing, Yun Liu; methodology and investigation, Liuyang Wang; writing—original draft preparation, Weijun Gao. All authors have read and agreed to the published version of the manuscript."

Acknowledgments

The authors acknowledge the Center of Analysis of Beijing University of Chemical Technology for FT-IR, EDX analyses.

Conflicts of interest

The authors declare no conflict of interest.

References

[1] L. Bulgariu, L.B. Escudero, O.S. Bello, M. Iqbal, J. Nisar, K.A. Adegoke, F. Alakhras, M. Kornaros, I. Anastopoulos, The utilization of leaf-based adsorbents for dyes removal: a review, J. Mol. Liq., 276 (2019) 728–747.
[2] V.K. Gupta, Suhas, Application of low-cost adsorbents for dye removal – a review, J. Environ. Manage., 90 (2009) 2313–2342.
[3] P. Zhang, D. O'Connor, Y. Wang, L. Jiang, T. Xia, L. Wang, D.C.W. Tsang, Y.S. Ok, D. Hou, A green biochar/iron oxide composite for Methylene blue removal, J. Hazard. Mater., 384 (2020) 121286, doi: 10.1016/j.jhazmat. 2019.121286.
[4] N. Supanchaiyamat, K. Jetsrisupar, J.T.N. Knijnenburg, D.C.W. Tsang, A.J. Hunt, Lignin materials for adsorption: current trend, perspectives and opportunities, Bioresour. Technol., 272 (2019) 570–581.
[5] P.J.M. Suhas, M.M.L. Carrott, R. Carrott, Lignin-from natural adsorbent to activated carbon: a review, Bioresour. Technol., 98 (2007) 2301–2312.
[6] D. Suteu, T. Malutan, D. Bilba, Removal of reactive dye Brilliant Red HE-3B from aqueous solutions by industrial lignin: equilibrium and kinetics modeling, Desalination, 255 (2010) 84–90.
[7] S. Zhang, Z. Wang, Y. Zhang, H. Pan, L. Tao, Adsorption of Methylene blue on organosolv lignin from rice straw, Procedia Environ. Sci., 31 (2016) 3–11.
[8] K. Fu, Q. Yue, B. Gao, Y. Sun, L. Zhu, Preparation, characterization and application of lignin-based activated carbon from black

liquor lignin by steam activation, Chem. Eng. J., 228 (2013) 1074–1082.
[9] A. Kriaa, N. Hamdi, E. Srasra, Adsorption studies of Methylene blue dye on Tunisian activated lignin, Russ. J. Phys. Chem. A, 85 (2016) 279–287.
[10] K. Mahmoudi, N. Hamdi, A. Kriaa, E. Srasra, Adsorption of methyl orange using activated carbon prepared from lignin by $ZnCl_2$ treatment, Russ. J. Phys. Chem. A, 86 (2012) 1294–1300.
[11] L.G. Silva, R. Ruggiero, P.M. Gontijo, R.B. Pinto, B. Royer, E.C. Lima, T.H.M. Fernandes, T. Calvete, Adsorption of Brilliant Red 2BE dye from water solutions by a chemically modified sugarcane bagasse lignin, Chem. Eng. J., 168 (2011) 620–628.
[12] M.A. Adebayo, L.D.T. Prola, E.C. Lima, M.J. Puchana-Roseroa, R. Cataluna, C. Saucier, C.S. Umpierres, J.C.P. Vaghetti, L.G. da Silva, R. Ruggiero, Adsorption of Procion blue MX-R dye from aqueous solutions by lignin chemically modified with aluminium and manganese, J. Hazard. Mater., 268 (2014) 43–50.
[13] J. Li, H. Li, Z. Yuan, J. Fang, L. Chang, H. Zhang, C. Li, Role of sulfonation in lignin-based material for adsorption removal of cationic dyes, Int. J. Biol. Macromol., 135 (2019) 1171–1181.
[14] W. Gao, J.P.W. Inwood, P. Fatehi, Sulfonation of hydroxymethylated lignin and its application, J. Bioresour. Bioprod., 4 (2019) 80–88.
[15] J. Geng, F. Gu, J. Chang, Fabrication of magnetic lignosulfonate using ultrasonic-assisted in situ synthesis for efficient removal of Cr(VI) and Rhodamine B from wastewater, J. Hazard. Mater., 375 (2019) 174–181.
[16] F. Gu, J. Geng, M. Li, J. Chang, Y. Cui, Synthesis of chitosan–ignosulfonate composite as an adsorbent for dyes and metal ions removal from wastewater, ACS Omega, 4 (2019) 21421–21430.
[17] H. Zhou, H. Xu, Y. Liu, Aerobic oxidation of 5-hydroxymethylfurfural to 2,5-furandicarboxylic acid using Co/Mn-Lignin coordination complexes-derived catalysts, Appl. Catal., B, 244 (2019) 965–973.
[18] H. Zhou, S. Hong, H. Zhang, Y. Chen, H. Xu, X. Wang, Z. Jiang, S. Chen, Y. Liu, Toward biomass-based single-atom catalysts and plastics: highly active single-atom Co on N-doped carbon for oxidative esterification of primary alcohols, Appl. Catal., B, 256 (2019) 117767, doi: 10.1016/j.apcatb.2019.117767.
[19] T.C.A. Siqueira, I.Z. da Silva, A.J. Rubio, R. Bergamasco, F. Gasparotto, E.A. de S. Paccola, N.U. Yamaguchi, Sugarcane bagasse as an efficient biosorbent for Methylene blue removal: kinetics, isotherms and thermodynamics, Int. J. Environ. Res., 17 (2020) 526, doi: 10.3390/ijerph17020526.
[20] I. Langmuir, The adsorption of gases on plane surfaces of glass, mica and platinum, J. Am. Chem. Soc., 40 (1918) 1361–1403.
[21] H. Freundlich, Über die Adsorption in Lösungen, Z. Phys. Chem., 57 (1906) 385–470.
[22] T.D. Minh, M.C. Ncibi, M. Certenais, M. Viitala, M. Sillanpää, Cobalt-lignosulfonate complex derived non-noble catalysts: facile valorization for high-performance redox conversion of organic pollutants, J. Cleaner Prod., 253 (2020) 120013, doi: 10.1016/j.jclepro.2020.120013.
[23] S. Islas-Valdez, S. López-Rayo, H. Hristov-Emilov, L. Hernández-Apaolaza, J.J. Lucena, Assessing metal–lignosulfonates as fertilizers using gel filtration chromatography and high-performance size exclusion chromatography, Int. J. Biol. Macromol., 142 (2020) 163–171.
[24] A. Maleki, U. Hamesadeghi, H. Daraei, B. Hayati, F. Najafi, G. McKay, R. Rezaee, Amine functionalized multi-walled carbon nanotubes: single and binary systems for high capacity dye removal, Chem. Eng. J., 313 (2017) 826–835.
[25] H.L. Chieng, L.B.L. Lim, N. Priyantha, Sorption characteristics of peat from Brunei Darussalam for the removal of Rhodamine B dye from aqueous solution: adsorption isotherms, thermodynamics, kinetics and regeneration studies, Desal. Water Treat., 55 (2015) 664–677.
[26] X. Li, Y. He, H. Sui, L. He, One-step fabrication of dual responsive lignin coated Fe_3O_4 nanoparticles for efficient removal of cationic and anionic dyes, Nanomaterials, 8 (2018) 162, doi: 10.3390/nano8030162.